Experimental Electron Temperature Gradient Dependence of Heavy Impurity Transport in Fusion Devices

D. Villegas, R. Guirlet, C. Bourdelle, G. T. Hoang, X. Garbet, and R. Sabot
CEA, IRFM, F-13108 Saint-Paul-lez-Durance, France
(Received 19 March 2010; published 13 July 2010)

The turbulent impurity (nickel) transport dependence on the normalized electron temperature gradient has been analyzed in sawtooth-free electron cyclotron wave heated Tore Supra plasmas. In the core, our experimental analysis shows that the lower R/L_{T_e}, the lower the nickel diffusion coefficient. The latter decreases until the instability threshold is reached. The experimental threshold is in agreement with the one computed by a gyrokinetic model. Further out, R/L_{T_e} plays no role in the impurity diffusion. This set of experimental results is consistent with a quasilinear gyrokinetic analysis.

DOI: 10.1103/PhysRevLett.105.035002 PACS numbers: 52.55.Fa, 52.25.Fi, 52.25.Vy, 52.35.Ra

Particle pinch is commonly observed in magnetized plasmas, despite homogenization due to diffusion processes. Turbulence is believed to be responsible for pinching processes, both in magnetosphere and plasma laboratory experiments [1]. In tokamaks, like ITER [2], fuel (deuterium and tritium) density peaking is favorable since it enhances fusion reactivity. On the other hand, impurity pinch is deleterious because of radiation losses and plasma dilution. Hence it is of prime importance to understand the mechanisms which control particle transport in fusion devices.

Beyond a threshold predicted by theoretical simulations, transport increases sharply as a function of the temperature and density gradients in both turbulence types [3]. These predictions have been validated experimentally in electron heat transport studies such as in ASDEX-Upgrade [4] and in Tore Supra [5].

Although impurity transport is an active field of research [6–8], such a turbulent threshold has not been observed so far. More generally speaking, experimental results validating the predicted diffusion contribution to the impurity flux $\Gamma = -D\nabla n + Vn$ driven by turbulence are sparse [9–12].

For the first time, we report in this Letter an experimental observation of the reduction of heavy impurity diffusion in the plasma core when the electron temperature gradient decreases towards the turbulent instability threshold. Further out, there is no R/L_{T_e} dependence. These results are consistent with a quasilinear gyrokinetic turbulent transport model.

To study the $\nabla T_e/T_e$ influence on impurity transport, we analyzed three sawtooth- and MHD-free circular Tore Supra [13] plasmas heated by 250 kW of electron cyclotron resonance continuous wave power in pure heating scheme (ECH). In two discharges, the same ECH power is injected at a different location: $r/a = 0.35$ or $r/a = 0.6$. In a third discharge, the same power is equally distributed between these two locations. The total injected power is kept constant for all discharges, as shown by the identical T_e profiles in the outer part of the plasma [see Fig. 1(a)]. The ECH configuration is such that it does not affect the measurements.

The electron temperature profiles are shown in Fig. 1(a) and the relevant gradients in Fig. 1(b). They are measured by a 32-channel electron cyclotron emission radiometer [14] with a 2.5 cm spatial sampling and 1 ms time sampling. The error bar on these profiles is about 3%. Consequently, the measurement error bar on the normalized electron temperature gradient calculated from a sta-

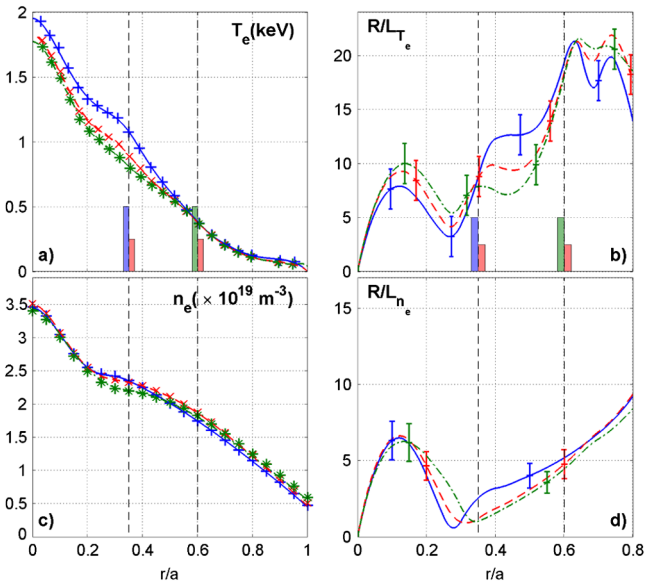

FIG. 1 (color online). Experimental profiles with ECH deposited at $r/a = 0.35$ in blue (+), at $r/a = 0.6$ in green (∗), and the mixed case in red (×). (a) Electron temperature T_e, (b) normalized electron temperature gradient $R/L_{T_e} = -R\nabla T_e/T_e$, (c) electron density n_e, and (d) normalized electron density gradient $R/L_{n_e} = -R\nabla n_e/n_e$. The black dashed vertical lines indicate the power deposition radii $r/a = 0.35$ and $r/a = 0.6$. The colored bars indicate the power fraction at either radius. Other plasmas parameters are $B_T = 3.78$ T, $I_p = 0.5$ MA, $P_{\mathrm{ECH}} = 250$ kW.

tistical method using the 3σ rule varies from 23% in the center to 15% at the edge. In the inner part of the plasma between $r/a = 0.1$ and $r/a = 0.5$, the T_e profile shape depends on the ECH power deposition radius: at $r/a = 0.1$, R/L_{T_e} is substantially changed from 7.5 to 10 as the power deposition location is shifted outwards.

The ion temperature T_i used in the gyrokinetic simulations is deduced from a charge exchange spectrometer.

The electron density $\langle n_e \rangle = 1.5 \times 10^{19}$ m^{-3} is measured by a 10-chord interferometer and two reflectometers [15,16]. The density profiles are displayed in Fig. 1(c) and their gradients in Fig. 1(d). The three profiles are the same within an error bar of 5%.

The impurity to be studied, nickel ($Z = 28$), is injected as a trace by a laser blowoff system described in [11]. The impurity behavior is observed with a set of diagnostics. A vacuum ultraviolet spectrometer consisting of a single line of sight in the midplane of the plasma measures the time evolution of the Ni XVII line at 24.92 nm, whose time evolution is used as the Ni source term in the transport simulations, and the Ni XXV line at 11.85 nm, emitted in the core plasma.

Two soft-x-ray cameras with a 2 ms time resolution provide information on impurity radiation in the plasma core. These cameras are equipped with a 50 μm thick Be filter. The corresponding cutoff energy is around 2 keV. One can find more details about these diagnostics in [11,12].

The radial transport code ITC [11] is used to perform the radial transport analysis. It solves the system of continuity equations coupling all the ionization stages of the injected impurity

$$\frac{\partial n_Z}{\partial t} + \vec{\nabla} \cdot \vec{\Gamma}_Z = S_{Z-1} + R_{Z+1} - (S_Z + R_Z) + s_{\text{ext}}$$

over the time interval during which the injected impurity is present in the plasma. S_k and R_k represent, respectively, the number of ionizations and recombinations of the ionization stage k of the impurity per time unit. $\vec{\Gamma}_Z = -D_Z(r)\vec{\nabla}n_Z(r) + \vec{V}_Z(r)n_Z(r)$ is the impurity flux and s_{ext} the external source of impurities. D_Z and V_Z are assumed to be time independent and unchanged for all ionization stages k. Positive V_Z corresponds to an outward convective flux. Despite a localized impurity injection point, the impurity distribution is poloidally uniform within $r/a < 0.85$. The Ni XVII emission located further inside ($r/a \approx 0.6$) is thus appropriate to represent the source term in ITC.

With an initial guess of D_Z and V_Z profiles, ITC solves the system of equations to obtain the radial density profile of each ionization stage of the impurity. Then, from the resulting impurity density profile it reconstructs the UV line and soft–x-ray brightnesses according to the geometry of these diagnostics. Finally, a minimization procedure based on the genetic algorithm PIKAIA [17] yields the transport coefficient profiles which best fit the experiment.

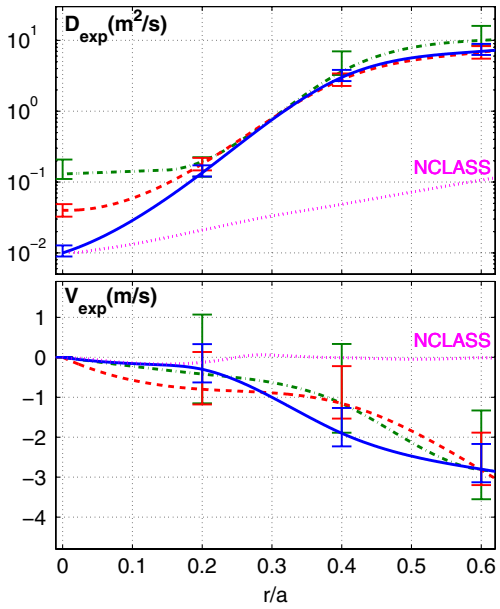

FIG. 2 (color online). Experimental radial profiles of D_Z and V_Z coefficients with error bars for the central deposition case in solid blue line, the mixed case in dashed red line, and the external deposition case in dash-dotted green line. The dashed pink lines correspond to NCLASS results.

The resulting transport coefficient profiles are presented in Fig. 2.

Depositing ECH at $r/a = 0.35$ leads to reduced diffusion in the plasma center ($D_Z \approx 0.01$ m^2/s for this innermost deposition case). In the core part of the plasma ($r/a \leq 0.2$), D_Z increases as the power deposition location is moved outward. For $r/a \geq 0.3$, the diffusion profiles of all ECH shots are very similar and diffusion increases up to the plasma edge.

As already noticed in [12], the determination of the convection velocity is subject to larger uncertainties. However, for all shots, V_Z is negative except in the plasma core where the uncertainty is large. This corresponds to inward convection everywhere in the plasma. In addition, the V_Z profiles are very similar in all cases within error bars.

These experimental profiles have been compared with the neoclassical transport coefficients computed with the CRONOS/NCLASS code package [18,19]. It takes into account the time evolution of the impurity density profiles of each ionization stage found with ITC. The uncertainties have been calculated according to the method explained in [12].

At the plasma center ($r/a < 0.05$), the experimental diffusion coefficient is very close to the neoclassical level in the innermost ECH deposition case. In the rest of the plasma, the experimental diffusion is unambiguously greater than the neoclassical one by at least 1 order of magnitude. This is a strong indication that turbulence plays

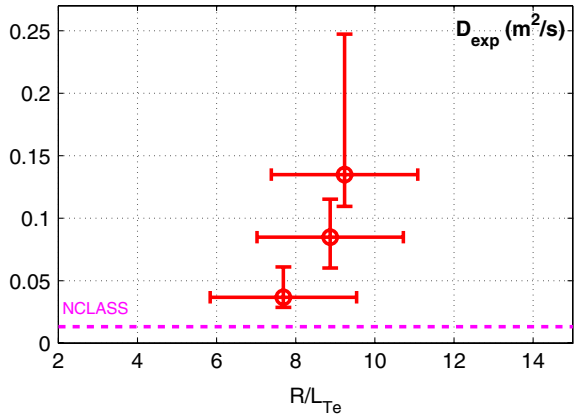

FIG. 3 (color online). Experimental diffusion (○) versus normalized electron temperature gradient R/L_{T_e} at $r/a = 0.1$. Other parameters are $R/L_{T_i} = 2.1$, $R/L_{n_e} = 6.4$, $T_e/T_i = 2.4$, $Z_{\text{eff}} = 1.7$, $q = 1.1$, $s = 0.3$.

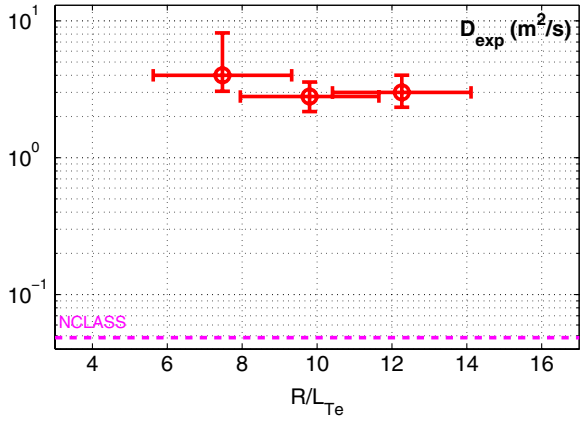

FIG. 4 (color online). Experimental diffusion (○) versus normalized electron temperature gradient R/L_{T_e} at $r/a = 0.4$. Other parameters are $R/L_{T_i} = 3.6$, $R/L_{n_e} = 2.5$, $T_e/T_i = 1.8$, $Z_{\text{eff}} = 1.7$, $q = 2.3$, $s = 0.9$.

a major role in the region beyond $r/a \geq 0.1$. As for convection, the results for the neoclassical convection velocity show a value close to 0, changing its sign, up to $r/a \approx 0.6$ where the convection becomes inward.

Comparing these results with the normalized electron temperature gradient in each case, we can notice that at $r/a = 0.1$ the diffusion coefficient increases steeply with the electron temperature gradient (cf. Fig. 3).

Although it was not possible to reach low enough values of R/L_{T_e} to observe the theoretical threshold of turbulence instabilities, it can be inferred from the experimental points that D_Z would decrease until it reaches the neoclassical level when the electron temperature gradient is equal to this threshold. If we plot a linear fit through the three experimental points of Fig. 3, we find an experimental estimate of the electron temperature gradient threshold $(R/L_{T_e})_c^{\text{exp}} \approx 6.9 \pm 2.4$.

On the contrary, at $r/a = 0.4$, the diffusion coefficient does not depend strongly on the electron temperature gradient (Fig. 4).

This difference can be understood in the frame of the theory of turbulent transport: using the same input as NCLASS, linear gyrokinetic calculations with the KINEZERO [20] and GYRO [21] code shows the existence of two regions: in the inner part of the plasma ($r/a < 0.15$) turbulence is found to be dominated by modes in the electron drift direction like trapped electron modes (TEM), which depend on the electron temperature gradient. Further out ($r/a > 0.25$), turbulence is dominated by ion temperature gradient modes (ITG).

The dependence of the diffusion coefficient on the electron temperature gradient (Fig. 5) has been computed with a quasilinear gyrokinetic fixed-gradient code named QUALIKIZ [22,23]. It provides absolute values of D and V. A comparison with the nonlinear gyrokinetic code GYRO [21] has shown that a single normalization factor is needed to reproduce GYRO results, for all parameters and for both heat and particle fluxes.

Nickel was considered to be fully stripped, which is a satisfactory assumption given the nickel charge state distribution in the plasma and the weak effect of the impurity charge found in [11,12]. In QUALIKIZ simulations, the effective charge of the plasma is assumed to be $Z_{\text{eff}} = 1.0$ to ensure that the impurity is a trace. With the experimental value of $Z_{\text{eff}} = 1.7$, the growth rate is reduced by at most 35%.

When turbulence is dominated by electron modes, the simulation results exhibit a variation of the diffusion coefficient with the electron temperature gradient consistent with the experimental results. Below the threshold $(R/L_{T_e})_c \approx 6$, D is neoclassical. Above it, D increases

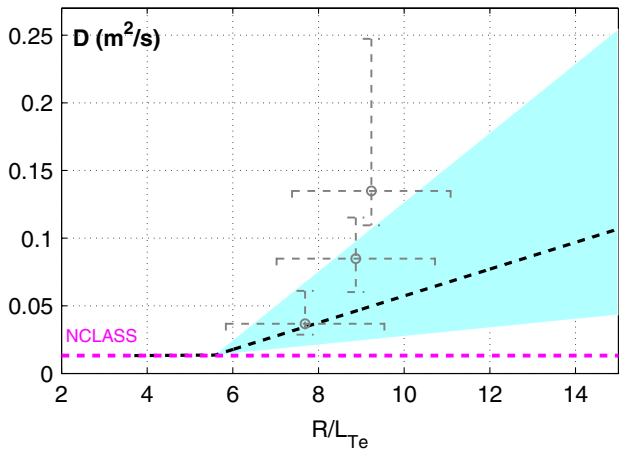

FIG. 5 (color online). QUALIKIZ diffusion versus normalized electron temperature gradient R/L_{T_e} at $r/a = 0.1$. The shaded light blue area corresponds to ion temperature gradient uncertainty. Experimental points are plotted in gray.

steeply. The QUALIKIZ threshold is in agreement with the experimental threshold considering the error bars.

These results explain the electron temperature gradient dependence: in the core part of the plasma, with TEM dominated turbulence, only electron temperature affects the transport characteristics. Further out, for $r/a \geq 0.25$, ITG modes are dominant. The fact that these modes are independent of the electron temperature explains the absence of dependence of the experimental D_Z on the electron temperature gradient.

Turbulent transport models predict that the impurity convection velocity is the sum of three terms [24]. The first one, called curvature pinch, is due to compressibility of the electric drift velocity in the inhomogeneous magnetic field. Directed inward, it only depends on the geometry and is usually the dominant contribution. The second term, the parallel compressibility caused by the parallel dynamics of impurities, is proportional to the ratio Z/A [25], Z being the impurity charge and A its mass number. As already said, the charge variation of nickel in the plasma is very weak. Thus, we can consider that the parallel compressibility does not vary and put together these two terms into a total curvature convection velocity V_{comp}. The third term, the so-called thermodiffusion (V_{thdiff}), depends on the temperature gradient $\nabla T/T$. The thermodiffusion sign can changed from outward to inward depending on the direction of fluctuations, i.e., preferentially outward for ITG and inward for TEM [26].

We have seen above that experimental convection velocity profiles V_Z do not depend on the gradient within error bars. This is due to a very weak thermodiffusion in the total convection velocity. In fact, using QUALIKIZ to estimate the relative weight between V_{thdiff} and V_{comp}, V_{thdiff} is found to be around $\approx$10% of the total convection velocity V_{tot}. As already shown in [26,27], the thermodiffusion is proportional to $1/Z$, where Z is the impurity charge. For nickel ($Z = 28$), it explains the absence of dependence of the experimental convection velocity. Hence, the convection velocity is dominated by the inward curvature term.

The influence of the normalized electron temperature gradient on impurity transport has been studied by varying the deposition location of electron cyclotron wave power. Nickel injections have been analyzed with our 1D impurity transport code. The experimental transport coefficient profiles, clearly above the neoclassical level, are in agreement with the calculated profiles within the uncertainties mainly due to the experimental error bars on the gradients.

In the core plasma ($r/a < 0.2$), experimental results show that above the instability threshold, the larger R/L_{T_e}, the larger the diffusion. Quasilinear gyrokinetic simulations, consistent with the experimental observation, find that the plasma is dominated by turbulent electron modes. The experimental results extrapolation is in agreement with the computed threshold. Further out, where turbulence is driven by ITG, the experimental diffusion does not depend on the electron temperature gradient.

Because of the $1/Z$ factor in the thermodiffusion convection velocity, no R/L_{T_e} dependence of the inward convection was found experimentally for heavy impurities.

This work, supported by the European Communities under the contract of Association between EURATOM and CEA, was carried out within the framework of the European Fusion Development Agreement. The views and opinions expressed herein do not necessarily reflect those of the European Commission.

[1] A. C. Boxer *et al.*, Nature Phys. **6**, 207 (2010).
[2] M. Shimada *et al.*, Nucl. Fusion **47**, S1 (2007).
[3] X. Garbet *et al.*, Plasma Phys. Controlled Fusion **46**, B557 (2004).
[4] F. Ryter *et al.*, Phys. Rev. Lett. **95**, 085001 (2005).
[5] G. T. Hoang *et al.*, Phys. Rev. Lett. **87**, 125001 (2001).
[6] R. Dux *et al.*, Plasma Phys. Controlled Fusion **45**, 1815 (2003).
[7] C. Giroud *et al.*, Nucl. Fusion **47**, 313 (2007).
[8] H. Takenaga *et al.*, Nucl. Fusion **43**, 1235 (2003).
[9] M. E. Puiatti *et al.*, Phys. Plasmas **13**, 042501 (2006).
[10] C. Angioni *et al.*, Plasma Phys. Controlled Fusion **49**, 2027 (2007).
[11] T. Parisot *et al.*, Plasma Phys. Controlled Fusion **50**, 055010 (2008).
[12] R. Guirlet *et al.*, Nucl. Fusion **49**, 055007 (2009).
[13] B. Saoutic *et al.*, Fusion Sci. Technol. **56**, 1079 (2009).
[14] J. L. Segui *et al.*, Rev. Sci. Instrum. **76**, 123501 (2005).
[15] R. Sabot *et al.*, Nucl. Fusion **46**, S685 (2006).
[16] F. Clairet *et al.*, Plasma Phys. Controlled Fusion **43**, 429 (2001).
[17] P. Charbonneau, Astrophys. J. Suppl. Ser. **101**, 309 (1995).
[18] J. F. Artaud *et al.*, Nucl. Fusion **50**, 043001 (2010).
[19] W. Houlberg *et al.*, Phys. Plasmas **4**, 3230 (1997).
[20] C. Bourdelle *et al.*, Nucl. Fusion **42**, 892 (2002).
[21] J. Candy and R. E. Waltz, Phys. Rev. Lett. **91**, 045001 (2003).
[22] A. Casati *et al.*, Nucl. Fusion **49**, 085012 (2009).
[23] A. Casati *et al.*, Phys. Rev. Lett. **102**, 165005 (2009).
[24] S. Futatani *et al.*, Phys. Rev. Lett. **104**, 015003 (2010).
[25] C. Angioni and A. G. Peeters, Phys. Rev. Lett. **96**, 095003 (2006).
[26] N. Dubuit *et al.*, Phys. Plasmas **14**, 042301 (2007).
[27] C. Bourdelle *et al.*, Phys. Plasmas **14**, 112501 (2007).